X-ray diffraction study of the smectic-$\tilde{A}$ fluid antiphase and its transitions to smectic-A_1 and smectic-A_2 phases

M. J. Young, Lei Wu,* G. Nounesis,† C. W. Garland, and R. J. Birgeneau
Center for Materials Science and Engineering and School of Science, Massachusetts Institute of Technology, Cambridge, Massachusetts 02139
(Received 18 January 1994)

A high-resolution x-ray diffraction study has been carried out on a binary liquid crystal mixture of pentylphenylcyanobenzoyloxy benzoate (DB_5CN) and cyanobenzoyloxypentyl stilbene (C_5 stilbene) that is 49.5 mole % C_5 stilbene. This mixture exhibits on cooling the phase sequence monolayer smectic-A (SmA_1)–smectic-A fluid antiphase ($Sm\tilde{A}$)–bilayer smectic-A (SmA_2). We observe the presence of a broad coexistence region between the $Sm\tilde{A}$ phase and the SmA_2 phase, contrary to previous work which reported a smectic-A crenelated phase. The behavior of the smectic-A fluid antiphase ordering and the evolution of the system to $Sm A_2$ order via a two-phase coexistence region are described in detail. Our results are compatible with previous high-resolution heat capacity measurements on the same sample.

PACS number(s): 64.70.Md, 61.30.−v, 64.60.Fr

I. INTRODUCTION

Thermotropic liquid crystal systems possess rich intermolecular and entropic interactions which allow for a multitude of ordered structures and a wide variety of order-disorder transitions [1]. In fact, smectic liquid crystalline order alone is realized in more than ten classes, the best known being the smectic-A phases. The simplest structure of this class is the monomeric smectic-A_m ($Sm A_m$), which can occur in nonpolar rodlike mesogenic molecules. Smectic-A polymorphism is typically observed in molecules with long (three-ring) aromatic cores and a polar head group which provides the molecule with a longitudinal dipole moment. Studies of mixtures of these dipolar mesogens have revealed a variety of interesting phases within the $Sm A$ class: In particular, the partial bilayer $Sm A_d$, the monolayer $Sm A_1$, the bilayer $Sm A_2$, and a more exotic biaxial phase intermediate between the latter two—the smectic-A fluid antiphase ($Sm\tilde{A}$) [2–6]. The hallmark of the $Sm\tilde{A}$ phase is the establishment of a long-period polarization wave within the layers [7–10].

It is known that for a range of concentrations, binary mixtures of the polar cyano mesogens pentylphenylcyanobenzoyloxy benzoate (DB_5CN) and cyanobenzoyloxypentyl stilbene (C_5 stilbene) exhibit a smectic fluid antiphase $Sm\tilde{A}$ between the $Sm A_1$ and $Sm A_2$ phases [3–5]. A partial phase diagram of this system is shown in Fig. 1. Depicted in Fig. 2 are real space sketches of several $Sm A$ structures including $Sm\tilde{A}$, which possesses a centered rectangular two-dimensional lattice with $m = a/2$ [7]. Reciprocal space pictures of the x-ray scattering associated with these structures are also shown in Fig. 2. $Sm\tilde{A}$ order is analogous to the antiphase domain order which occurs in binary alloys. It consists of two dimensionally ordered slabs; hence, this phase is characterized by the usual density modulation normal to the layers and an in-plane wave vector modulated at $q_\perp = q_T^0$, where $q_\perp$ is the transverse component in (q_H, q_K, q_L) space.

It has been reported that yet another smectic-A fluid antiphase intermediate between the $Sm\tilde{A}$ phase and the $Sm A_2$ phase occurs for these systems, and this has been designated as crenelated smectic-A or $Sm A_{cren}$ [7]. The $Sm A_{cren}$ phase differs from the $Sm\tilde{A}$ phase in its in-plane order. In essence, the periodic antiphase domains are proposed to be slabs of different thicknesses with $m < a/2$, while the longitudinal order remains unchanged (see Fig. 2). We will show that the region of the

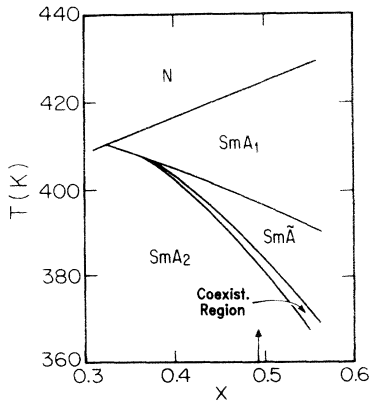

FIG. 1. Partial phase diagram for mixtures of DB_5CN and C_5 stilbene, taken from Ref. [4]. The narrow region labeled "coexist region" was formerly assigned to the $Sm A_{cren}$ phase but is now ascribed to a broad coexistence of $Sm\tilde{A}$ and $Sm A_2$ phases. X denotes the mole fraction of C_5 stilbene, and the arrow indicates the composition studied in this work.

*Present address: General Atomic, San Diego, CA 92121.
†Present address: Francis Bitter National Magnet Laboratory, Massachusetts Institute of Technology, Cambridge, MA 02139.

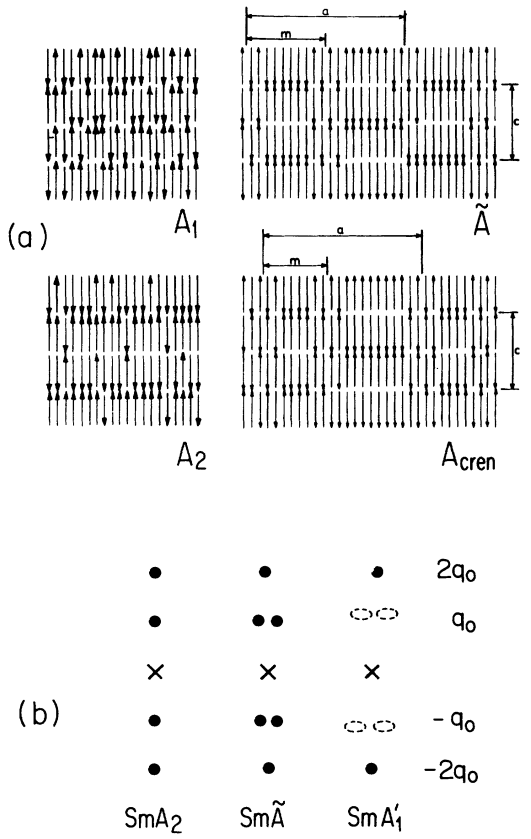

FIG. 2. (a) Schematic structures for monolayer SmA_1, bilayer SmA_2, and the fluid antiphase $Sm\tilde{A}$ (a centered rectangular structure with $m=a/2$); also shown is a structure for the purported SmA_{cren} phase where $m<a/2$. (b) The corresponding reciprocal space x-ray scattering patterns. The dashed elliptical areas represent diffuse scattering due to short-range fluctuations.

phase diagram for DB_5CN and C_5 stilbene between the $Sm\tilde{A}$ and SmA_2 phases corresponds to a broad two-phase coexistence region, as opposed to a new type of smectic-A fluid antiphase.

This paper is organized as follows: First, a description of the experimental apparatus and the sample is given in Sec. II. Results for the SmA_1 phase with its concomitant $Sm\tilde{A}$ fluctuations, the $Sm\tilde{A}$ phase, the SmA_2 phase, and the $Sm\tilde{A}+SmA_2$ two-phase coexistence region will be presented in Sec. III. A discussion comparing our results with previous heat capacity, optical and electron microscopy, and x-ray diffraction experiments will be given in Sec. IV.

II. EXPERIMENTAL DETAILS

Pentylphenylcyanobenzoyloxy benzoate (DB_5CN) and cyanobenzoyloxypentyl stilbene (C_5 stilbene) have the following molecular formulas:

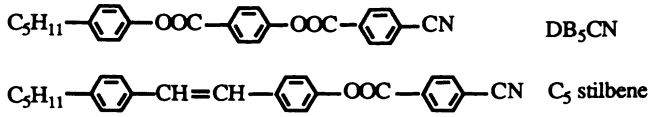

with molecular masses of 413.48 and 395.50 g, respectively. These compounds were synthesized and purified at the Centre de Recherche Paul Pascal [3], and they are from the same batch that was used for an earlier C_p investigation [11]. The x-ray sample is a mixture with C_5 stilbene mole fraction $X=0.495$, which was previously used for a high-resolution x-ray study of critical fluctuations in the nematic (N) phase near the N-SmA_1 transition [12]. The phase sequence for this sample is

$$SmA_2 \underset{382-384.4\ K}{\leftrightarrow} Sm\tilde{A} \underset{\sim 397\ K}{\leftrightarrow} SmA_1 \underset{424.0\ K}{\leftrightarrow} N$$

where 382–384.4 K represents a broad $Sm\tilde{A}+SmA_2$ coexistence range. The transition temperatures cited above are slightly lower than those reported previously [11,12] due to a slow drift (approximately -32 mK/day) in transition temperatures with time over the very long period (60 days) of x-ray observations.

The experiment was conducted using Cu $K\alpha$ radiation from a Rigaku model RU-300 rotating-anode machine operating at 7 kW and a triple-axis spectrometer with Si(111) monochromator and analyzer crystals set in a dispersive configuration. The instrumental resolution for the in-plane longitudinal direction was well approximated by a Lorentzian with a half width at half maximum (HWHM) of 1.4×10^{-4} Å^{-1}. The transverse in-plane resolution was considered perfect ($<10^{-5}$ Å^{-1}), while the transverse out-of-plane resolution was well approximated by a Gaussian with a HWHM of 0.03 Å^{-1} and was set by incoming and outgoing slits with matching angular acceptance. Evacuated flight paths with narrow slits positioned before and after the sample reduced the background count rate to 0.25 counts per second. The beam had a spot size of 1.5×3 mm^2 at the sample position.

A sample of mass 180 mg was sealed with indium in a beryllium cell $12\times12\times1.5$ mm^3. This cell was placed in a two-stage oven constructed from two beryllium cylinders which were individually temperature controlled throughout the experiment to ±10 mK. The sample was aligned in the nematic (N) phase in a 5.5-kG magnetic field by cycling slowly across the N-SmA_1 transition until the sharpest transverse scan was obtained. With this technique it was possible to obtain a sample mosaicity of 0.5° HWHM in the SmA_1 phase in the vicinity of the N-SmA_1 transition.

III. RESULTS

The SmA_1 phase is characterized by a sinusoidal one-dimensional mass density wave in a three-dimensional fluid. Short-range, fluidlike order between molecules is observed in the direction transverse to this density wave. As is well known, the SmA_1 ordering gives rise in an x-ray scattering experiment to a single quasi-Bragg peak at $(0,0,2q_0)$. For DB_5CN and C_5 stilbene in the N phase near the N-SmA_1 transition, $2q_0=0.2481$ Å^{-1}, which equals $2\pi/L$ with an effective molecular length L of 25.33 Å [12]. This value is consistent with Levelut *et al.* [3], who report that L is close to the value 26.8 Å for this system with $X=0.46$, the small difference being mainly due to slightly different mole fractions X. Well below the N-

SmA_1 transition, SmA_1 monolayer type order is well established; hence, changes in the mosaic are gradual and there is no measurable change in the resolution-limited longitudinal $2q_0$ linewidth with temperature. However, despite this essentially "frozen" smectic-A_1 order, there are fluctuations of in-plane domain order [7,8] which become larger with decreasing temperature. From ac calorimetry measurements on this mixture [11], we know that the SmA_1-Sm$\tilde{A}$ transition is accompanied by significant pretransitional energy fluctuations over a large range in temperature, indicative of the presence of short-range Sm$\tilde{A}$-like order in the SmA_1 phase.

In the x-ray experiment these Sm$\tilde{A}$ fluctuations are demonstrated by the appearance of weak diffuse spots off-axis which were first detectable about 7 K above the SmA_1-Sm$\tilde{A}$ transition temperature. Figure 3(a) shows five transverse scans along $(q_\perp,0,q_0)$ at temperatures within the SmA_1 phase and two scans in the Sm$\tilde{A}$ phase. Figure 3(b) shows the corresponding longitudinal scans in which q_L is varied, with q_H held fixed at q_T^0. The diffuse scattering data were fitted with the empirical form first suggested by Chen and Lubensky [13] for the N-SmC transition:

$$\sigma(\mathbf{q})=\frac{\sigma_0}{1+B(q_\parallel-q_0)^2+Cq_\perp^2+Dq_\perp^4}\ , \tag{1}$$

where $q_\parallel$ is the L component and $q_\perp$ is the H component of the scattering vector in (q_H,q_K,q_L) space and the quadratic coefficient C is negative. The results of these fits are shown in Fig. 3. Following Martinez-Miranda, Kortan, and Birgeneau [14], we have defined length scales using the half width at half maxima of the peaks, which correspond to the size of the smectic-A fluid antiphase domains:

$$\xi_\parallel(q_T^0)=\left[\frac{B}{1+\frac{1}{2}C(q_T^0)^2}\right]^{1/2}, \tag{2}$$

$$\xi_\perp(q_T^0)=\frac{\sqrt{2D}}{\left\{-C+\left[C^2+4D\left[\frac{1-C^2}{2D}\right]\right]^{1/2}\right\}^{1/2}-\sqrt{-C}}\ , \tag{3}$$

where $q_T^0=(-C/2D)^{1/2}$ is the peak wave vector in the transverse direction. Below the SmA_1-Sm$\tilde{A}$ transition, these off-axis diffuse peaks become resolution limited in radial scans, thus confirming long-range order in the Sm$\tilde{A}$ phase. Pure transverse scans in the scattering plane reveal a mosaic with a roughly Gaussian angular distribution.

The size of the modulation repeat distance $\underline{a}=2\pi/q_T^0$ increases on cooling, which is clearly shown in Fig. 3(a) by the change in q_T^0, the off-axis peak position of the $(q_\perp,0,q_0)$ scans. The monotonic trend of the in-plane modulation distance $\underline{a}$ with temperature is indicated by the variation of q_T^0 shown in Fig. 4(a). The value of q_T^0 decreases on cooling to 0.020 Å^{-1} (corresponding to $\underline{a}$= 315 Å) at the point where two-phase Sm$\tilde{A}$+SmA_2 coexistence begins. The smooth curve through the q_T^0-T

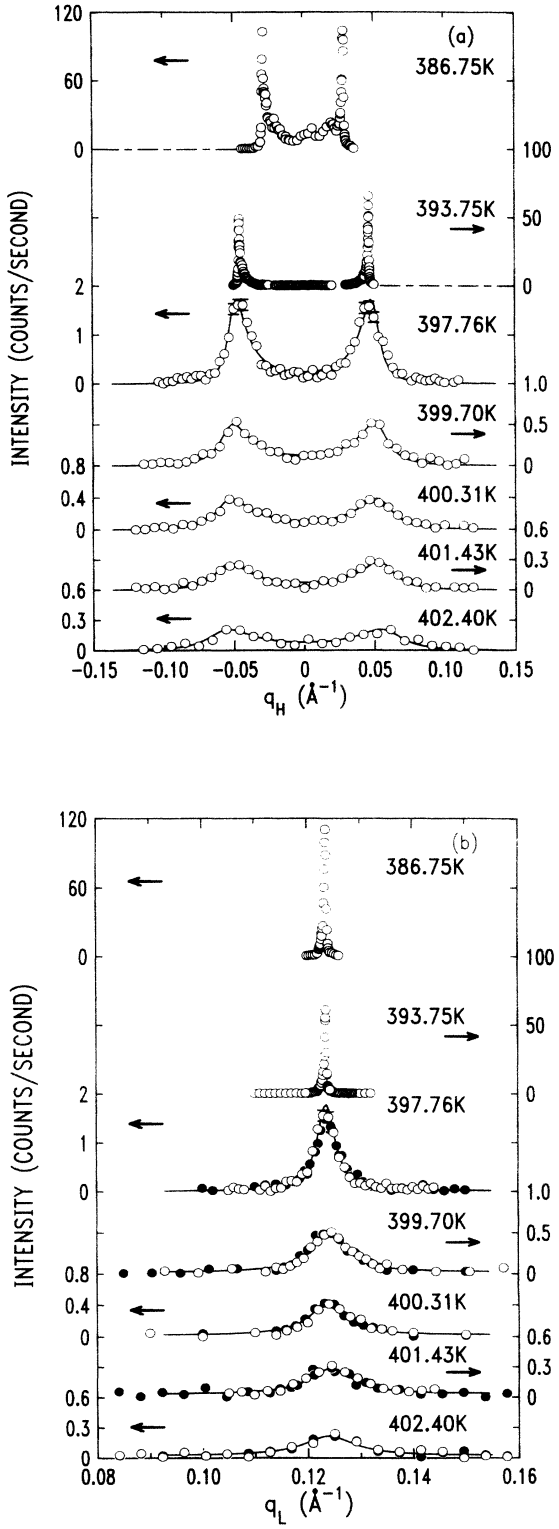

FIG. 3. (a) Scans along q_H with $q_L=q_0$ in the SmA_1 and Sm$\tilde{A}$ phases. (b) Scans varying q_L with $q_H=q_T^0$ in the SmA_1 and Sm$\tilde{A}$ phases. The open circles are for data along $(+q_T^0,0,q_L)$ and the solid circles are for $(-q_T^0,0,q_L)$. The five scans at $T>396$ K are in the SmA_1 phase, and the diffuse peaks are fitted with Eq. (1). The arrows indicate the intensity scale associated with each scan. The two scans at $T<396$ K are in the Sm$\tilde{A}$ phase.

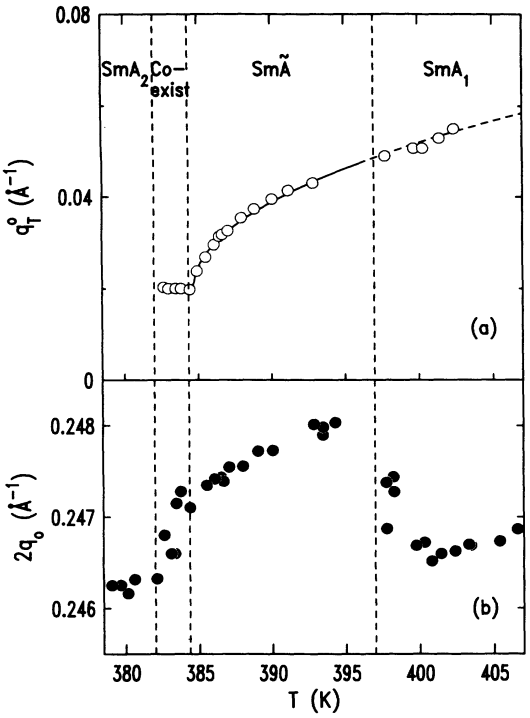

FIG. 4. Scattering wave vectors for DB_5CN and C_5 stilbene: (a) Transverse position q_T^0 of the off-axis $(\pm q_T^0,0,q_0)$ peaks in the Sm$\tilde{A}$ and SmA_1 phases. The smooth curve through these q_T^0 points in the Sm$\tilde{A}$ phase has the empirical form $(q_T^0-0.02)=0.01\ (T-384.4)^{1/2}$, and the dashed curve in the SmA_1 phase is an extrapolation of this form to higher T. (b) Longitudinal position of the $(0,0,2q_0)$ peak across the entire range of temperature for this experiment.

data in the Sm$\tilde{A}$ phase represents an empirical fit with the quadratic form

$$(q_T^0-0.02)=0.01(T-384.4)^{1/2}\ .$$

Note that this formula when extrapolated to higher temperatures is still in good agreement with the q_T^0 values determined from diffuse off-axis peaks in the SmA_1 phase.

The position of the $(0,0,2q_0)$ peak, shown in Fig. 4(b), changes linearly with T in the Sm$\tilde{A}$ phase and in the SmA_1 phase above ~400 K. An extrapolation of these SmA_1 values to 426 K yields $2q_0=0.2479$ Å^{-1}; this is in good agreement with the value $2q_0=0.2481$ Å^{-1} determined from the diffuse SmA_1 scattering in the nematic phase [12]. One can see from Fig. 4(b) that near the SmA_1-Sm$\tilde{A}$ transition, there is a noticeable deviation from the monotonic increase in $2q_0$ with temperature, probably due to greater "dimerization" in the fluid antiphase than in the SmA_1 phase. The scatter in the data points in this region is due to uncertainties in both $\Delta T=T-T_c(A_1-\tilde{A})$ due to T_c drifts and $2q_0$ resolution ($\pm 1\times 10^{-4}$ Å^{-1}). The values of q_0 for the off-axis $(q_T^0,0,q_0)$ peaks have also been determined as a function of temperature. For the diffuse peaks in the SmA_1 phase, we find that $(q_0)>\frac{1}{2}(2q_0)$, where $(2q_0)$ is determined from the position of the $(0,0,2q_0)$ Bragg peak; the ratio $(q_0)/(2q_0)$ ranged from 0.5041 at 402.40 K to 0.5010 at 397.76 K. In the Sm$\tilde{A}$ phase and in the SmA_2+Sm$\tilde{A}$ coexistence region, we found $(q_0)/(2q_0)=0.5$ within our resolution (± 0.0007) for all temperatures. These observations are in agreement with those reported by Levelut [7].

The peak intensities I_T of the off-axis diffuse scattering in the SmA_1 phase are shown in Fig. 5(a). Finally, the correlation lengths $\xi_\perp$ and $\xi_\parallel$ determined from the diffuse $(q_T^0,0,q_0)$ peaks using Eqs. (1)–(3) are shown in Fig. 5(b). The uncertainties in these ξ values are moderately large, but note that $\xi_\parallel$ and $\xi_\perp$ only differ by a factor of ~2.2.

Before considering the Sm$\tilde{A}$+SmA_2 coexistence region, let us first describe the low temperature SmA_2 phase. The SmA_2 bilayer phase occurs when antiferroelectrically aligned molecular dimers form a double layer structure, as shown in Fig. 2. The reciprocal space picture is described by fundamental scattering centered at $(0,0,q_0)$ and second harmonic scattering centered at $(0,0,2q_0)$ [15]. Fluidlike order within the SmA_2 layers is present as in the SmA_1 phase, and there is no off-axis $(q_T^0,0,q_0)$ scattering in the SmA_2 phase.

In the temperature range 382–384.4 K between the Sm$\tilde{A}$ phase region and the SmA_2 phase region, a detailed study was made of the scattering profiles for off-axis $(\pm q_T^0,0,q_0)$ peaks and on-axis $(0,0,q_0)$ and $(0,0,2q_0)$ peaks. This is the temperature region where a new modulated structure, the SmA_{cren} phase with a regular

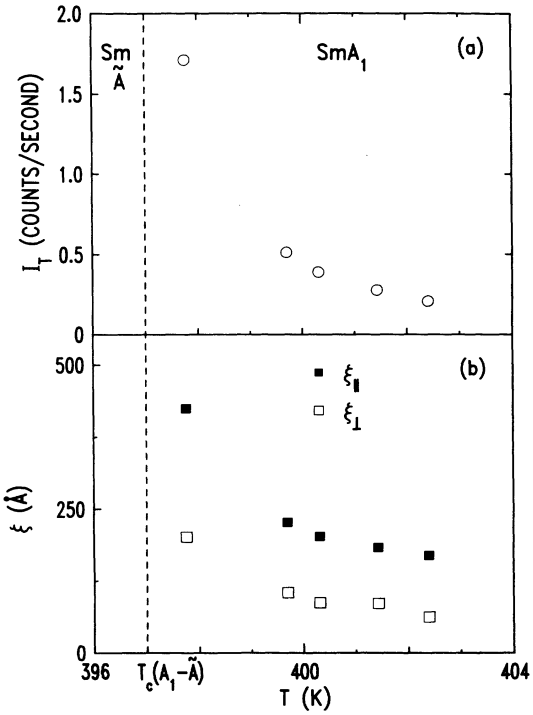

FIG. 5. Intensity and correlation length data for diffuse $(q_T^0,0,q_0)$ off-axis peaks in the SmA_1 phase: (a) Peak intensities I_T (○) and (b) longitudinal and transverse correlation lengths $\xi_\parallel$ (■) and $\xi_\perp$ (□) for the in-plane modulation obtained from Eqs. (2) and (3) and fits to the off-axis scattering profile with Eq. (1).

array of two different thickness antiphase slabs with $m < a/2$, has been proposed to exist [7]. Contrary to that description, our results demonstrate that the transformation between the Sm$\tilde{A}$ and SmA_2 phases occurs via a broad two-phase coexistence region. Figure 6 shows θ rocking curves through the $(0,0,q_0)$ peak as a function of T. Figure 7 shows the temperature variation of the intensity for $(q_T^0,0,q_0)$ off-axis and $(0,0,q_0)$ on-axis peaks over the coexistence range where Sm$\tilde{A}$ transforms into SmA_2. As the system is cooled through the two-phase coexistence region, the q_T^0 and q_0 positions of the off-axis $(q_T^0,0,q_0)$ peak do not change but the intensity of this peak decreases smoothly. At the same time, the intensity of the on-axis $(0,0,q_0)$ peak grows, as shown by both Figs. 6 and 7. This behavior is exactly what one would expect if domains of SmA_2 phase appear with decreasing temperature at the expense of the domains of Sm$\tilde{A}$.

The presence of two separate types of ordered structure, SmA_2 and Sm$\tilde{A}$, is evident by comparing the mosaics of the on-axis and off-axis peaks. A contour plot of the scattering intensities observed in the coexistence region is shown in Fig. 8. If the scattering were produced by a single ordered phase, there would be only one mosaic distribution as measured from θ rocking curves. However, the dramatic difference between the angular widths of the on-axis $(0,0,q_0)$ and off-axis $(\pm q_T^0,0,q_0)$ peaks rules out the possibility of a single phase. We should point out that scattering at $(0,0,2q_0)$ can result from both SmA_2 and Sm$\tilde{A}$ ordered domains, so both contributions must be considered in the analysis of that mosaic. Figure 9

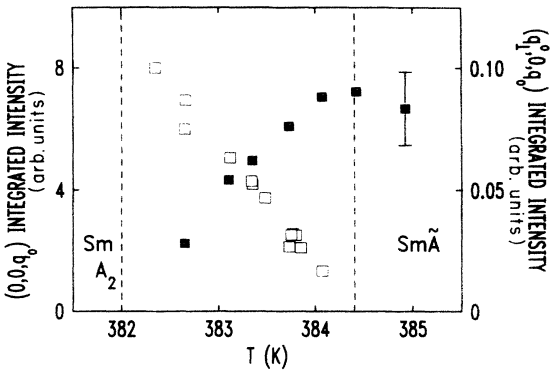

FIG. 7. Detail of x-ray intensity data in the Sm$\tilde{A}$+SmA_2 coexistence region. The integrated intensities of the $(0,0,q_0)$ bilayer peak (□) and the $(q_T^0,0,q_0)$ fluid antiphase peak (■) are shown.

shows mosaic data at two temperatures within the coexistence region. At $T=383.35$ K we observe the mosaics of the off-axis $(\pm q_T^0,0,q_0)$ peaks to be consistent with the on-axis $(0,0,2q_0)$ mosaic but strikingly different from the on-axis $(0,0,q_0)$ mosaic. This is to be expected since Fig. 7 shows that the integrated intensity of the $(0,0,q_0)$ peak at this temperature is weak relative to its saturation value below 382 K. Hence, the SmA_2 contribution at $(0,0,2q_0)$

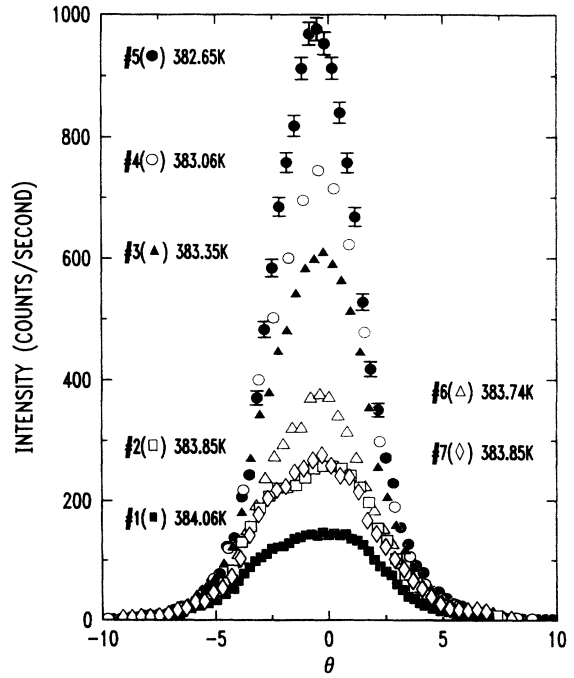

FIG. 6. θ rocking curves at constant radial wave vector through the $(0,0,q_0)$ peak in the Sm$\tilde{A}$+SmA_2 coexistence region. The run numbers 1–7 are in chronological order, i.e., the sample was first cooled (1–5) and then reheated (6 and 7).

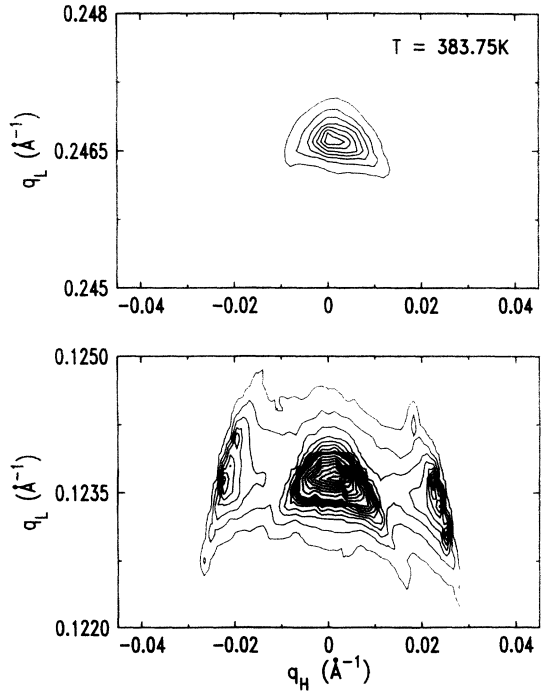

FIG. 8. Contour plot of scattering intensities observed at 383.75 K in the Sm$\tilde{A}$+SmA_2 coexistence region. Features at $(\pm q_T^0,0,q_0)$ arise from Sm$\tilde{A}$ scattering, that at $(0,0,q_0)$ from SmA_2 scattering, and that at $(0,0,2q_0)$ from both Sm$\tilde{A}$ and SmA_2 scattering. Note the mosaic broadening of the off-axis $(q_T^0,0,q_0)$ peaks.

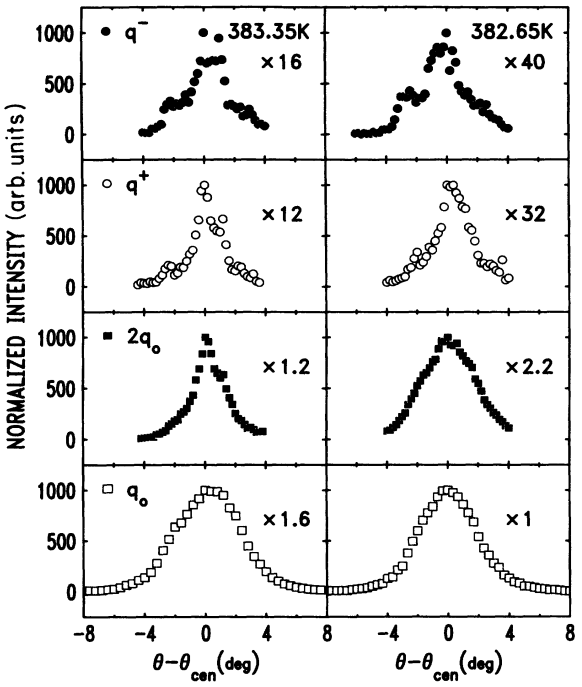

FIG. 9. Comparison of mosaicity widths in the $SmA_2+Sm\tilde{A}$ coexistence region at $T=383.35$ (left panel) and 382.65 K (right panel) during a slow cooling run. q^+ and q^- are the off-axis peaks centered at $(0.022\ \text{Å}^{-1},0,q_0)$ and $(-0.022\ \text{Å}^{-1},0,q_0)$, respectively; q_0 is the on-axis $(0,0,q_0)$ bilayer peak; $2q_0$ is the on-axis $(0,0,2q_0)$ peak with contributions from both $Sm\tilde{A}$ and SmA_2 scattering. The factor by which I (experimental) was multiplied to obtain the normalized intensity is given for each scan.

will be qualitatively insignificant. In contrast to this, SmA_2 domains are quite large compared to $Sm\tilde{A}$ domains at $T=382.65$ K, as seen from the integrated intensities shown in Fig. 7. Thus, their contribution to the scattering at $(0,0,2q_0)$ should be quite substantial, resulting in a q_0-like mosaic for the $(0,0,2q_0)$ peak, as observed. However, the mosaic of the $(0,0,q_0)$ peak remains distinctly different from the mosaics at $(+q_T^0,0,q_0)$ and $(-q_T^0,0,q_0)$. One can observe noticeable differences not only between the absolute angular widths of the mosaics but also between the features in each peak. Since these features do not reflect the symmetry of reciprocal space, they can be attributed to the mosaicity, probably originating from domains which lack perfect azimuthal symmetry about the scattering vector $\mathbf{q}=(0,0,q)$. This is expected, given that our spectrometer is configured to integrate over a wide out-of-plane momentum transfer. This comparison of the two off-axis peaks with the two on-axis peaks shows clearly the presence of two distinct mosaics. More precisely, we observe the disappearance of $Sm\tilde{A}$ ordered domains with the simultaneous development of SmA_2 ordered domains on cooling through a ~2.4-K-wide coexistence region.

The final experiment designed to distinguish $Sm\tilde{A}+SmA_2$ coexistence from a SmA_{cren} phase involved scans through the off-axis harmonics $(\pm nq_T^0,0,q_0)$ of the $Sm\tilde{A}$ fundamental $(\pm q_T^0,0,q_0)$. The data shown in Fig. 10 were obtained at 383.75 K, which is in the coexistence region. In addition to observing the large on-axis $(0,0,q_0)$ peak and the off-axis $(q_T^0=0.022\ \text{Å}^{-1},0,q_0)$ peak, we made a careful search at the $(2q_T^0,0,q_0)$ and $(3q_T^0,0,q_0)$ positions. Long counting time scans were used in order to achieve a good signal-to-noise ratio in these regions of weak scattering. The third harmonic is observed at $(+0.066,0,q_0)$, but there is no indication of the second harmonic at $(2q_T^0,0,q_0)$. It should be noted that the latter is not allowed by symmetry even in multiple scattering for either the $Sm\tilde{A}$ or SmA_2 phases separately but could occur in a two-phase coexistence region via double scattering between domains of each phase. Such $(\pm 2q_T^0,0,q_0)$ peaks were indeed reported in Ref. [7] and were interpreted as evidence of a SmA_{cren} ordered structure. The relatively weak integrated intensity of the third harmonic peak in our data compared to the fundamental allows us to ascribe a nearly pure sinusoidal shape to the polarization modulation transverse to the smectic mass

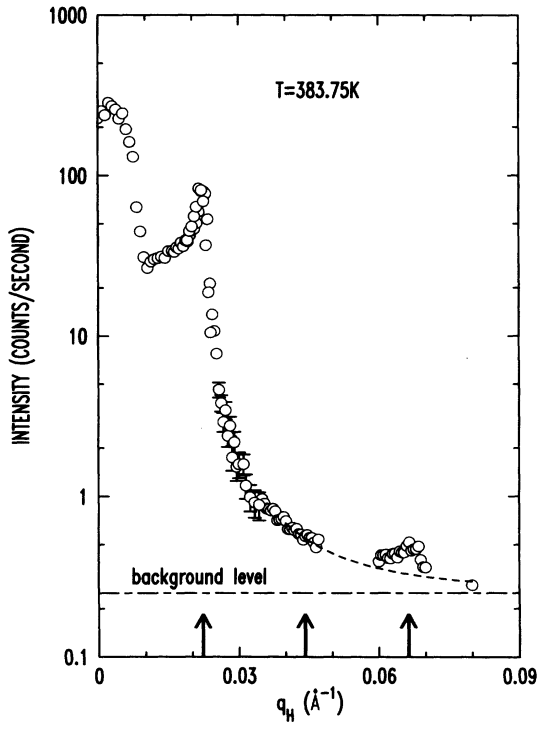

FIG. 10. Third harmonic $(3q_T^0,0,q_0)$ at $q_H=0.066\ \text{Å}^{-1}$ compared to the fundamental $(q_T^0,0,q_0)$ at $q_H=0.022\ \text{Å}^{-1}$ showing that the $Sm\tilde{A}$ phase in a $Sm\tilde{A}+SmA_2$ coexistence mixture exhibits a nearly sinusoidal polarization wave transverse to the smectic mass density wave. Note that the second harmonic at $(0.044,0,q_0)$ is not allowed by symmetry for a $Sm\tilde{A}+SmA_2$ two-phase mixture and is not observed within our resolution. The error bars for points with $q_H>0.035$ are comparable to the size of the symbols since long counting times were employed. The dashed curve for $q_H>0.048\ \text{Å}^{-1}$ represents the large q_H scattering expected in part due to long tails for the fundamental peak and in part due to mosaic broadening.

density wave. Thus, the fluid antiphase domains are separated by broad domain walls even when Sm$\tilde{A}$ ordering is as fully developed as possible and Sm$\tilde{A}$ coexists with the SmA_2 phase.

It should be noted that for the run during which the data of Figs. 7–10 were obtained, the lateral position q_T^0 of the off-axis $(\pm q_T^0, 0, q_0)$ peaks was $q_T^0 = 0.022$ Å^{-1} instead of 0.02 Å^{-1} as observed in the run shown in Fig. 4. Such slight variations in the maximum $\underline{a}$ value observed in the coexistence region from run to run are of no conceptual importance.

IV. DISCUSSION

This section will present a discussion of five issues: the fluctuations of Sm$\tilde{A}$-like short-range order in the SmA_1 phase, the nature of the SmA_1-Sm$\tilde{A}$ transition, the evolution of long-range lateral modulations in the Sm$\tilde{A}$ phase, the two-phase coexistence region associated with the Sm$\tilde{A}$-SmA_2 transition, and the scattering behavior at q_0 and $2q_0$ in the SmA_2 phase.

A. Fluctuations in the Sm A_1 phase

The presence of in-plane Sm$\tilde{A}$-like fluctuations in a SmA_1 phase has been detected previously in x-ray [7,9], viscosity [3], and calorimetry [11] studies. The detailed behavior of the pretransitional energy fluctuations for both DB_5CN and C_5 stilbene and DB_6CN and C_5 stilbene mixtures is shown in Fig. 11. It is clear from this figure that ΔC_p^+ data above $T_c(A_1\text{-}\tilde{A})$ do not follow a simple power-law behavior, but the qualitative trend in the experimental ΔC_p values is similar to that predicted from a "weak crystallization" theory of the SmA_1-Sm$\tilde{A}$ transition [16]. Although the present x-ray data shown in Fig. 5 for $(q_\perp, 0, q_0)$ scans in the SmA_1 phase are too sparse to test power-law analyses of $\xi_\parallel$ and $\xi_\perp$, one can make a consistency check between the behavior of ΔC_p^+ and the correlation lengths.

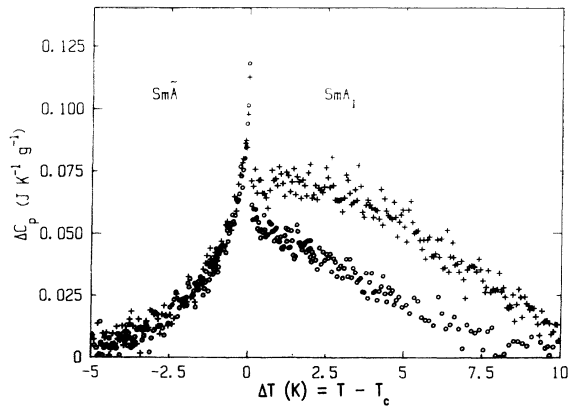

FIG. 11. Excess heat capacity associated with the SmA_1-Sm$\tilde{A}$ transition [11]. The open circles are data for DB_5CN and C_5 stilbene with $X=0.492$ and the plus signs are data for DB_6CN and C_5 stilbene with $X=0.505$. The transition temperature is denoted as T_c although the transition is very weakly first order.

The concept of two-scale universality states that $\bar{F}\xi_{\rm vol}/k_BT$, where $\bar{F}_c$ is the critical free energy per unit volume and $\xi_{\rm vol}$ is the correlation volume, should be a dimensionless constant for a given universality class [17]. In the present case, the correlation length in the y direction is unknown but can be assumed to vary with T in the same way as $\xi_\perp$ does. Thus one expects for Sm$\tilde{A}$ fluctuations,

$$\bar{F}_c \xi_\parallel \xi_\perp^2 / T = C \ , \tag{4}$$

where C is a constant independent of T. Integrating the ΔC_p^+ data in Fig. 11 to obtain $\bar{F}_c$ as a function of ΔT and choosing the x-ray transition temperature to be 397 K (see Fig. 5), we obtain $C=-1.7$ at 397.76 K, -2.8 at 399.70 K, -2.4 at 400.31 K, -2.9 at 401.43 K, and -2.6 at 402.40 K. The fact that C is roughly constant while $\xi_\parallel \xi_\perp^2$ and $\bar{F}_c$ are each varying by a factor of ~ 20 is an indication of consistency between the ΔC_p^+ data and our diffuse x-ray scattering results.

Another test of internal consistency for the Sm$\tilde{A}$ fluctuation behavior is to consider the ratio $\xi_\parallel \xi_\perp / I_T$. If simple power-law behaviors $\xi \sim (\Delta T)^{-\nu}$ and $I \sim (\Delta T)^{-\gamma}$ were to hold, this ratio would vary as $(\Delta T)^{\eta\nu}$, almost independent of ΔT, since scaling gives $\gamma = (2-\eta)\nu$ and $\eta \ll 1$. For the five data points shown in Fig. 5, we obtain an approximately constant value for this ratio, which demonstrates that I_T indeed scales like $\xi_\parallel \xi_\perp$.

It should also be noted that in the SmA_1 phase $(q_0) > 0.5(2q_0)$, where (q_0) is the L component of the off-axis $(q_T^0, 0, q_0)$ diffuse peak and $(2q_0)$ is that of the on-axis $(0,0,2q_0)$ condensed peak. The ratio $(q_0)/(2q_0)$ locks in at 0.5 at the SmA_1-Sm$\tilde{A}$ transition temperature.

B. The Sm A_1-Sm $\tilde{A}$ transition

According to a mean-field treatment of the frustrated smectics model, the SmA_1-Sm$\tilde{A}$ transition would be second order, but fluctuation effects of the Brazovskii type make this transition first order [16,18]. This is confirmed by the heat capacity measurements, which indicate a weakly first-order transition with a coexistence region of ~ 85 mK [11]. No x-ray data were obtained close to the SmA_1-Sm$\tilde{A}$ transition temperature, but Fig. 4 suggests that very little change occurs in $\underline{a} = 2\pi/q_T^0$ on going from the SmA_1 to Sm$\tilde{A}$ phase, which is consistent with any first-order discontinuity being small.

C. Evolution of lateral modulations in the Sm $\tilde{A}$ phase

The highest temperature x-ray data in the Sm$\tilde{A}$ phase were obtained at 393.75 K. The nearly resolution-limited off-axis peaks shown in Fig. 3 indicate that lateral modulation extends a considerable distance at that temperature. Although there is no theory dealing with fluctuation behavior at the SmA_1-Sm$\tilde{A}$ transition, Fig. 11 shows that energy fluctuations are large and distinctly different above and below $T_c = T_c(A_1\text{-}\tilde{A})$. The ΔC_p^- data below T_c can be well described by

$$\Delta C_p^- = A \ln(|\Delta T|/T_c) + B \ ,$$

with $A=-0.0224\ \mathrm{J\,K^{-1}\,g^{-1}}$ and $B=-0.096\ \mathrm{J\,K^{-1}g^{-1}}$, suggesting XY-like fluctuations.

In the middle of the Sm$\tilde{A}$ phase, say, 388–394 K, the lateral dimension of the Sm$\tilde{A}$ domains remains essentially unchanged. The mosaic spread of the off-axis peaks broadens significantly on cooling, but the integrated intensity I_T remains nearly constant, in agreement with an almost constant C_p across this temperature range [11]. Throughout the entire Sm$\tilde{A}$ phase, q_T^0 evolves in a smooth systematic way, until the lateral period $\underline{a}=2\pi/q_T^0$ reaches a maximum value of 315 Å, in reasonable agreement with the value 335 Å given by Levelut [7] for DB_6CN and C_5 stilbene. Electron micrographs of a freeze-fractured DB_5CN and C_5 stilbene mixture with $X=0.63$ show a very clear lateral periodicity of 400–500 Å [5] This is consistent with our value since $\underline{a}$ appears to increase as X increases and the Sm$\tilde{A}$ phase range shifts to lower temperatures [5,7]. The quadratic form

$$(q_T^0-0.02)=0.01(T-384.4)^{1/2}$$

found to represent the temperature dependence of q_T^0 is an empirical rather than a theoretically predicted result.

As the Sm$\tilde{A}$ phase is cooled toward the transition region where conversion into SmA_2 occurs, the integrated intensity I_T increases substantially. This qualitative trend in I_T is parallel to that in the heat capacity shown in Fig. 12. These C_p data represent a truncated version of the inverted Landau Sm$\tilde{C}$-SmC_2 heat capacity peak observed in DB_8ONO_2 and $DB_{10}ONO_2$ mixtures of alkyloxyphenyl-nitrobenzoyloxy benzoates [19]. In the latter case, the first-order coexistence region is only 0.17 K wide, whereas the C_p data in Fig. 12 indicate a broad two-phase coexistence region of ~2.2 K.

Note that the ratio $(q_0)/(2q_0)$ for the L components of the off-axis $(q_x,0,q_0)$ and on-axis $(0,0,2q_0)$ peaks equals 0.5 in the Sm$\tilde{A}$ phase. There is a systematic linear increase in $2q_0$ on cooling throughout the Sm$\tilde{A}$ phase followed by a very rapid decrease in $2q_0$ on the transition into the SmA_2 phase, as shown in Fig. 4.

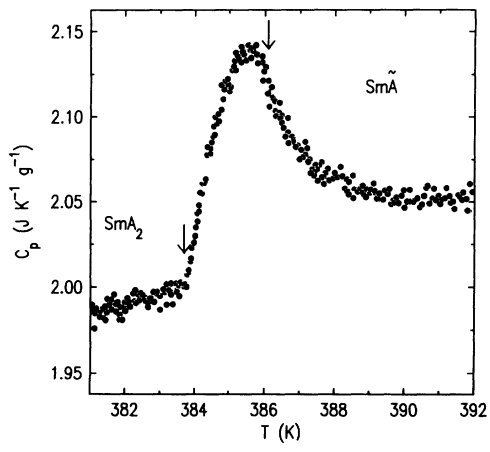

FIG. 12. Heat capacity associated with the Sm$\tilde{A}$ to SmA_2 transformation in DB_5CN and C_5 stilbene [11]. A broad two-phase coexistence region exists for temperatures between the two arrows.

D. The Sm$\tilde{A}$+SmA_2 coexistence region

For a DB_5CN and C_5 stilbene mixture with $X\simeq 0.5$, it was previously reported that another modulated smectic-A phase, denoted SmA_{cren}, which has the structure shown in Fig. 2, exists between the Sm$\tilde{A}$ and SmA_2 phases [7]. In contrast to this, we find that the 382–384.4 K range corresponds to a broad two-phase coexistence region. Levelut's key argument [7] for the existence of a SmA_{cren} phase instead of Sm$\tilde{A}$+SmA_2 coexistence was the presence of the $(2q_T^0,0,q_0)$ harmonic of the off-axis $(q_T^0,0,q_0)$ fundamental since even harmonics are not allowed by symmetry for the Sm$\tilde{A}$ and SmA_2 phases separately. However, as shown by Fig. 10, we see no $(2q_T^0,0,q_0)$ peak although a weak $(3q_T^0,0,q_0)$ peak was detected. Furthermore, the mosaic structure in Fig. 9, as discussed in Sec. III, strongly supports the presence of two separate coexisting phases. It seems that the situation here is very similar to the recent demonstration that a proposed incommensurate smectic-A phase SmA_{inc}, existing between the SmA_d and SmA_2 phases, is in fact a broad coexistence of SmA_d+SmA_2 phases that interconvert very slowly [20]. As noted previously, the observation of weak $(\pm 2q_T^0,0,q_0)$ peaks could possibly be explained by double scattering between two domains in a Sm$\tilde{A}$+SmA_2 coexistence mixture. We should point out, however, that, according to Levelut [21], her photographically detected diffraction patterns are inconsistent with this explanation and the observed scattering in her experiment necessitates the existence of an intrinsic SmA_{cren} phase. We can only state definitively that the SmA_{cren} phase was not observed in our experiment.

The existence of a first-order Sm$\tilde{A}$-SmA_2 transition is consistent with the predictions of Prost's frustrated smectic model [10,22], which does not yield a SmA_{cren} phase for any set of model parameters. Sluggish two-phase coexistence is also compatible with the heat capacity results shown in Fig. 12. Indeed, Ref. [11] describes the C_p behavior between the two arrows as being "like a special type of two-phase coexistence," and the small phase shift anomaly $\Delta\phi$ reported in Ref. [11] for the T_{ac} signal could well be due to the motion of domain walls between Sm$\tilde{A}$ and SmA_2 regions rather than antiphase SmA_{cren} domain walls. Finally, the microscopic observation of transient textures in this region [4] can be as well explained by two-phase coexistence as by a SmA_{cren} phase [23].

E. The smectic-A_2 phase

In the SmA_2 phase there are only the two on-axis peaks at q_0 and $2q_0$, both slightly mosaic broadened in the same way. At 376.3 K, which is ~6.9 K below the midpoint of the Sm$\tilde{A}$+SmA_2 coexistence range and ~48 K below the N-SmA_1 transition, the ratio of intensities $I(2q_0)/I(q_0)$ is 0.3. This value can be compared with $I(2q_0)/I(q_0)$ ratios of 0.07 at $\Delta T=T-T_{NA_2}=-2$ K in 7APCBB and ~0.2 at $\Delta T\simeq -20$ K in DB_6CN [15].

Since the DB_5CN and C_5 stilbene mixture forms a $Sm A_2$ phase from already well-ordered $Sm\tilde{A}$ antiphase domains, one would expect temperature independent values of $I(q_0)$ and $I(2q_0)$, as observed, and a $I(2q_0)/I(q_0)$ ratio which reflects a saturation value comparable to that deep in the $Sm A_2$ phase for materials undergoing a N-$Sm A_2$ transition.

ACKNOWLEDGMENTS

The authors wish to thank H. T. Nguyen for synthesizing the liquid crystal samples and would also like to thank S. Kumar, A. M. Levelut, J. Prost, and G. Sigaud for helpful discussions. This work was supported by National Science Foundation Grant No. DMR 90-22933.

[1] *Phase Transitions in Liquid Crystals,* Vol. 290 of *NATO Advanced Study Institute, Series B: Physics,* edited by S. Martellucci and A. N. Chester (Plenum, New York, 1992).

[2] F. Hardouin, A. M. Levelut, J. J. Benattar, and G. Sigaud, Solid State Commun. **33**, 337 (1980); F. Hardouin, A. M. Levelut, M. F. Achard, and G. Sigaud, J. Chim. Phys. **30**, 53 (1983).

[3] G. Sigaud, F. Hardouin, M. F. Achard, and A. M. Levelut, J. Phys. (Paris) **42**, 107 (1981); A. M. Levelut, R. J. Tarento, F. Hardouin, M. F. Achard, and G. Sigaud, Phys. Rev. A **24**, 2180 (1981).

[4] G. Sigaud, F. Hardouin, and M. F. Achard, Phys. Rev. A **31**, 547 (1985).

[5] G. Sigaud, M. Mercier, and H. Gasparoux, Phys. Rev. A **32**, 1282 (1985).

[6] C. W. Garland, in *Geometry and Thermodynamics,* Vol. 229 of *NATO Advanced Study Institute, Series B: Physics,* edited by J.-C. Toledano (Plenum, New York, 1990), pp. 221–254.

[7] A. M. Levelut, J. Phys. (Paris) Lett. **45**, L603 (1984).

[8] C. R. Safinya, W. A. Varady, L. Y. Chiang, and P. Dimon, Phys. Rev. Lett. **57**, 432 (1986).

[9] B. I. Ostrovskii and M. A. Saidachmetov, Mol. Cryst. Liq. Cryst. **192**, 19 (1990).

[10] P. Barois, J. Pommier, and J. Prost, in *Solitons in Liquid Crystals,* edited by Lui Lam and Jacques Prost (Springer-Verlag, New York, 1989), Chap. 6.

[11] K. Ema, C. W. Garland, G. Sigaud, and Nguyen Huu Tinh, Phys. Rev. A **39**, 1369 (1989).

[12] C. W. Garland, G. Nounesis, M. J. Young, and R. J. Birgeneau, Phys. Rev. E **47**, 1918 (1993); note that the value $2q_0 = 0.2115$ Å^{-1} cited therein is a typographical error; the correct value is $2q_0 = 0.2481$ Å^{-1}.

[13] J. C. Chen and T. C. Lubensky, Phys. Rev. A **14**, 1202 (1976).

[14] L. J. Marinez-Miranda, A. R. Kortan, and R. J. Birgeneau, Phys. Rev. A **36**, 2372 (1987).

[15] K. K. Chan, P. S. Pershan, L. B. Sorensen, and F. Hardouin, Phys. Rev. A **34**, 1420 (1986); L. Wu, M. J. Young, Y. Shao, C. W. Garland, R. J. Birgeneau, and G. Heppke, Phys. Rev. Lett. **72**, 376 (1994).

[16] V. V. Lebedev and A. R. Muratov, J. Phys. II **1**, 135 (1991).

[17] D. Stauffer, M. Ferer, and M. Wortis, Phys. Rev. Lett. **29**, 345 (1972).

[18] J. Prost and P. Barois, J. Chim. Phys. **80**, 65 (1983); J. Wang and T. C. Lubensky, J. Phys. (France) **45**, 1653 (1984).

[19] K. Ema, G. Nounesis, C. W. Garland, and R. Shashidhar, Phys. Rev. A **39**, 2599 (1989).

[20] S. Kumar, L. Chen, and V. Surendranath, Phys. Rev. Lett. **67**, 322 (1991).

[21] A. M. Levelut (private communication).

[22] P. Barois, C. Coulon, and J. Prost, J. Phys. (Paris) Lett. **42**, L107 (1981).

[23] G. Sigaud (private communication). See also G. Sigaud, M. F. Achard, and F. Hardouin, J. Phys. (Paris) Lett. **46**, L825 (1985).